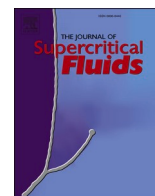




Since January 2020 Elsevier has created a COVID-19 resource centre with free information in English and Mandarin on the novel coronavirus COVID-19. The COVID-19 resource centre is hosted on Elsevier Connect, the company's public news and information website.

Elsevier hereby grants permission to make all its COVID-19-related research that is available on the COVID-19 resource centre - including this research content - immediately available in PubMed Central and other publicly funded repositories, such as the WHO COVID database with rights for unrestricted research re-use and analyses in any form or by any means with acknowledgement of the original source. These permissions are granted for free by Elsevier for as long as the COVID-19 resource centre remains active.



Solubility of favipiravir (as an anti-COVID-19) in supercritical carbon dioxide: An experimental analysis and thermodynamic modeling

Seyed Ali Sajadian^{a,b,*}, Nedasadat Saadati Ardestani^c, Nadia Esfandiari^d, Mahshid Askarizadeh^d, Abolghasem Jouyban^{e,f}

^a South Zagros Oil and Gas Production, National Iranian Oil Company, 7135717991 Shiraz, Iran

^b Department of Chemical Engineering, Faculty of Engineering, University of Kashan, 87317-53153 Kashan, Iran

^c Department of Nanotechnology and Advanced Materials, Materials and Energy Research Center, 14155-4777 Karaj, Iran

^d Department of Chemical Engineering, Marvdasht Branch, Islamic Azad University, Marvdasht, Iran

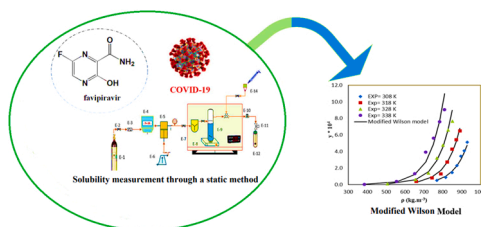
^e Pharmaceutical Analysis Research Center and Faculty of Pharmacy, Tabriz University of Medical Sciences, Tabriz, Iran

^f Faculty of Pharmacy, Near East University, PO BOX: 99138, Mersin 10, Nicosia, North Cyprus, Turkey

HIGHLIGHTS

- First report on solubility of favipiravir in supercritical carbon dioxide.
- Solubility data were correlated by density-based models.
- Effects of pressure and temperature were investigated on the solubility.
- Modified Wilson and K-J model can more accurately correlate experimental data.

GRAPHICAL ABSTRACT



ARTICLE INFO

Keywords:

Favipiravir solubility
Supercritical carbon dioxide (SC-CO₂)
Empirical model
Equation of state (EoS)
Expanded liquid theory
Simulated annealing

ABSTRACT

Favipiravir is one of the most commonly prescribed drugs in the treatment of COVID-19 in the early stages of the disease. In this work, the solubility of favipiravir was measured in supercritical CO₂ at temperatures ranging from 308 to 338 K and pressures ranging from 12 to 30 MPa. The mole fraction solubility of favipiravir was in the range of 3.0×10^{-6} to 9.05×10^{-4} . The solubility data were correlated with three types of methods including; (a) density-based models (Chrastil, Garlapati and Madras, Sparks et al., Sodeifian et al., K-J and Keshmiri et al.), (b) Equations of states SRK with quadratic mixing rules) and (c) expanded liquid theory (modified Wilson model). According to the results, modified Wilson and K-J models are generally capable of providing good correlation of solubility. Finally, the approximate values of total (ΔH_{total}), vaporization (ΔH_{vap}), and solvation (ΔH_{sol}) enthalpies were computed.

1. Introduction

In December 2019, a new coronavirus (COVID-19) emerged whose quick outbreak led to a pandemic according to the World Health

Organization (WHO) classification. COVID-19 was initially discovered in Wuhan, Hubei Province, China. Coronavirus can cause drastic acute respiratory syndrome (SARSCoV-2) [1]. SARS CoV-2 belongs to the coronaviridae family with a positive-strand RNA (+RNA) genome. An RNA-dependent RNA polymerase (RdRp) and proteases are encoded by

* Corresponding author at: South Zagros Oil and Gas Production, National Iranian Oil Company, 7135717991 Shiraz, Iran.

E-mail address: seyedalij.sajadian@gmail.com (S.A. Sajadian).

<https://doi.org/10.1016/j.supflu.2022.105539>

Received 16 November 2021; Received in revised form 31 January 2022; Accepted 1 February 2022

Available online 4 February 2022

0896-8446/© 2022 Elsevier B.V. All rights reserved.

Nomenclature

$a_0 - a_5$	Adjustable parameters of model
AARD%	Average absolute relative deviation
$a(T)$	Energy parameter of the cubic EoS ($\text{Nm}^4 \text{mol}^{-2}$)
B	Volume parameter for equations of state ($\text{m}^3 \text{mol}^{-1}$)
C	Solubility of solute (g/L)
c_s	Concentration of solute (g/L) in the collection vial
H_f^2	Molar heat of fusion
K_{ij}	Binary interaction parameter
K_{ij}	Binary interaction parameter in the mixing rules
L_{ij}	Binary interaction parameter in the mixing rules
M_w	Solute molecular weight (g/mol)
M_{CO_2}	CO ₂ molecular weight (g/mol)
N	Number of data points, dimensionless
P	Pressure
P_c	Critical pressure
Pr	Reduced pressure
P_{ref}	Reference pressure
P_{sub}	Sublimation pressure (Pa)
Q	Number of independent variables
R	Gas constant, $\text{Jmol}^{-1} \text{K}^{-1}$
R_{adj}	Adjusted correlation coefficient
S	Equilibrium solubility
T	Temperature, K
T_b	Boiling point
T_c	Critical temperature
T_r	Reduced temperature
y_2	Mole fraction solubility

V_s	Volume of the collection vial (L)
V_L	Volume of the sampling loop (L)
v^s	Solid molar volume
Z	Number of adjustable parameters

Greek symbols

$\alpha(Tr, \omega)$	Temperature-dependent function of the considered parameter of the EoS
α	Regressed parameter of the Wilson's model
β	Regressed parameter of the Wilson's model
δ	Solubility parameter (cal/cm^3) ^{0.5}
ρ	Density, kg.m^{-3}
ρ_c	Critical density
ρ_r	Reduced density
ρ_{ref}	Reference density
v_1, v_2	Volumes of the SCF and the solid solute, respectively
λ	Energies of interaction between the molecules designated in the subscripts
γ_2^∞	The activity coefficient of the solid solute at infinite dilution
Φ	Fugacity coefficient
w	Acentric factor

Superscripts

Cal	Calculated
Exp	Experimental
i, j	Component
Sub	Sublimation

this single-stranded RNA beta-coronavirus [2]. Quarantine and antiviral medicines significantly reduced the ultimate size of the prevalence and peak incidence [3]. Favipiravir, remdesivir, umifenovir, oseltamivir, immune globulin, lopinavir, azithromycin, and ivermectin have been employed for the treatment of COVID-19 [4].

Favipiravir (FAV) was endorsed by the Food and Drug Administration (FDA) in 2014 to cure new and re-emerging influenza viruses [3]. Thanks to their antiviral features, favipiravir and its derivatives have been approved as a prodrug and support in the treatment of the influenza virus [5]. FAV belongs to class II in the Biopharmaceutics Classification System (BCS). High permeability and low water solubility are two major characteristics of favipiravir. The poor solubility of the favipiravir in the aqueous media of the human body has decreased its effectiveness and bioavailability [6]. Recently, Abd Elkodous et al. [4] reviewed nanomaterial-based drug delivery systems for the treatment of COVID-19 to increase the bioavailability of current drugs, reduce their toxicity, and increase their efficiency. They reported that favipiravir-encapsulated nano-emulsions as prospective carriers of COVID-19 drug delivery. Biodegradable nano-emulsions have a kinetically persistent structure and can be dispersed both in oil and water. Small particles with a diameter range of 5–200 nm make up nano-emulsion formulae.

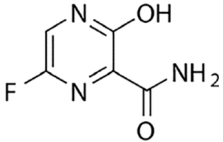
Various approaches have been developed to enhance the aqueous solubility and bioavailability of drugs among which, co-crystallization, salt formation, encapsulation/impregnation, and particle size reduction in micro/nano-scale can be mentioned. Furthermore, supercritical fluid technology could be a viable option to overcome the drawbacks of conventional techniques for enhancing the solubility of poor water-soluble formulas. Traditional processes suffer from temperature sensitivity and impurity contamination. Non-toxicity, eco-friendliness, and adaptability are among the benefits of SCF technology, making it an ideal route in green chemistry. SCF has been used to improve solubility

and increase the bioavailability of poorly soluble drugs [7–10]. The bioavailability of drugs is highly dependent on their solubility and dissolution. In this regard, the production of nano/microparticles of drugs through the SCF method is of paramount significance. Concerning particle development, SCF technology is an alternative technique for particle production which can avoid most of the disadvantages associated with conventional approaches such as crushing, milling, crystallization, and precipitation. More advanced technologies, such as microencapsulation, coating, and composite particle creation, can be developed by SCF technology [11–18]. The solubility of drugs in SC-CO₂ is the main parameter I reduction of the particle size, highlighting the significance of measuring drug solubility. Several methods have been introduced for the measurement of solubility among which, gravimetric, spectrometric, chromatographic, and miscellaneous methods can be mentioned.

Experimental measurement of drug solubility in SC-CO₂ at different temperatures and pressures is time-consuming, costly, and in some cases impossible. Therefore, various correlative models such as the equation of states (EoSs; (e.g. Peng-Robinson (PR) and Soave-Redlich-Kowang (SRK)), empirical models, and expanded liquid models (e.g. universal quasi-chemical (UNIQUAC) and modified Wilson's models) have been considered to correlate the solubility of solid at different pressures and temperatures in SC-CO₂. Prediction and correlation via EoS and expanded liquid require the calculation of the physicochemical properties of solid (pharmaceutical components) such as acentric factor, critical pressure, temperature, and sublimation pressure. These properties are not in literature and are usually determined by different group contribution (GC) methods. In return, the empirical models (density-based model), only require pressure, temperature, and SC-CO₂ density. The correlative model has indicated the best fitting with the experimental data [8,9,13,19].

In the current research, the solubility of favipiravir was measured in

Table 1
Structure and details of favipiravir.

Compound	Formula	CAS number	Structure	M_w (g/mol)	T_m (K)	λ_{max} (nm)
Favipiravir	$C_5H_4FN_3O_2$	259793–96–9		157.1	465.9	323

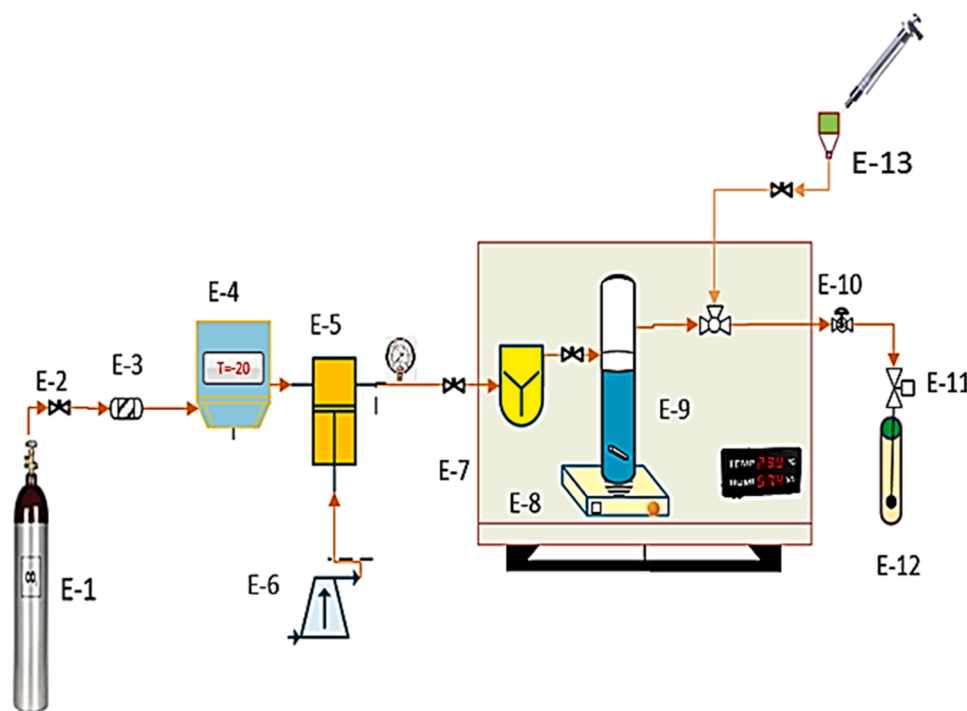


Fig. 1. Process diagram of experimental apparatus used for measuring favipiravir solubility. E-1: CO₂ cylinder, E-2: Needle valve, E-3: Filter, E-4: Refrigerator unit, E-5: High-pressure pump, E-6: Compressor, E-7: Oven, E-8: Magnetic stirrer, E-9: Equilibrium cell, E-10: Backpressure valve, E-11: Micrometer valve, E-12: Collection vial, E-13: syringe.

the temperature range of 308 – 338 K and the pressure range of 12 – 30 MPa. For this purpose, solubility data were correlated with three types of methods including (1) Empirical density-based models (Chrastil, Garlapati and Madras, Sparks et al., Sodeifian et al., K-J, and Keshmiri et al.) (2) Equations of states (EoSs) (Soave–Redlich–Kwong (SRK) with vdW2 mixing rule), and (3) expanded liquid theory (modified Wilson model). The mentioned models were evaluated based on mean absolute deviation (AARD%) and adjusted correlation coefficient (R_{adj}).

2. Experiments

2.1. Materials

Favipiravir (CAS No. 259793–96–9) has been procured through the Tofigh Darou pharmaceutical corporation (Tehran, Iran), at the minimum purity of 99%. Carbon dioxide (CO₂) was prepared by Oxygen Novin Company (Shiraz, Iran) with a purity of 99.99%. Analytical-grade methanol was supplied by Merck (Darmstadt, Germany). The structure of favipiravir (drug) and the information of all components are presented in Table 1.

2.2. Experimental apparatus

The applied laboratory setup with a spectrophotometer is presented

in Fig. 1 which encompassed a CO₂ cylinder (E-1), a needle valve (E-2), a molecular sieve filter (E-3), a refrigerator unit (E-4), a high-pressure pump (E-5, air driven liquid pump, type-M64, Shineeast Co., Shandong, China), an air compressor (E-6), an incubator (E-7, shimaz), magnetic stirrer (100 rpm) (E-8, Alfa, D-500 180,), a high-pressure equilibrium cell (E-9), a back-pressure valve (E-10, Xi'an Shelok Instrument Technology Co., Shaanxi, China), a micrometer valve (E-11), a collection vial (E-12), a Syringe (E-13). In this high-pressure system, all equipment, piping and connections were made from stainless steel 316 at 1/8" in size. The CO₂ flow from the cylinder first enters the molecular sieve filter (pore size of 1 μ m) to prevent impurities. It then flows to the refrigerator. The temperature inside the refrigerator is about – 15 °C, liquifying the CO₂ flow. The liquid CO₂ at the pressure in the CO₂ tank (about 60 bar) entered the high-pressure reciprocating pump. Using the pressure gauge and transmitter, measurements were performed at a precision of ± 1 bar.

In the next step, 3000 mg favipiravir was mixed in SC-CO₂ using a magnetic stirrer to establish an equilibrium phase into a cell with a capacity of 300 mL. The temperature was maintained at the desired level by an oven equipped with a digital display with temperature measurements at an accuracy of ± 0.1 K. A sintered filter (1 μ m) was used on both sides of the cell to hold the drug. Carbon dioxide was pressurized and then transferred to the cell at the appropriate pressure. The static time, i.e. the time to reach equilibrium, was considered 120 min based on the preliminary experiments. After 120 min, 600 μ L of

Table 2
Critical and physicochemical properties of favipiravir.

Component	T_b (K)	T_c (k)	P_c (bar)	ω	V_s (cm ³ /mol)	T (K)			
						308	318	328	338
Favipiravir	589.73 ^b	878.71 ^b	66.82 ^b	0.5799 ^c	97.53 ^d	2.43×10^{-8}	8.86×10^{-8}	2.94×10^{-7}	9×10^{-7}
Carbon dioxide		304.18	73.8	0.224					

^a Estimated by Grain-Watson method.

^b Marrero and Gani.

^c Estimated by the Ambrose–Walton corresponding states method.

^d Estimated by Immirzi–Perini method.

saturated SC-CO₂ was introduced into the injection loop using a three-valve two-position device. By redirecting the injection valve, the loop was depressurized into the collection vial containing a certain volume of methanol (solvent). In this part, the micrometer valve was used for controlling the flow.

In the final step, about 1 mL of solvent was injected through an external needle valve for washing the loop and the solution is collected in the vial. The final volume of the solution was 5 mL. Each experiment was repeated three times (triplicates). The favipiravir solubility values were determined by measuring the absorbance at λ_{max} on a Shimadzu UV-Vis spectrophotometer with a 1 cm long quartz cell. The solubility was calculated from the concentration of solute using the calibration curve (with regression coefficient 0.998) and the UV-absorbance.

At different sets of temperature and pressure, the equilibrium mole fraction, y_2 , and solubility, S (g/L), in SC-CO₂ were computed as follows [20]:

$$y_2 = \frac{n_{solute}}{n_{solute} + n_{CO_2}} \quad (1)$$

where:

$$n_{solute} = \frac{C_s \left(\frac{g}{L}\right) V_s(L)}{M_s \left(\frac{g}{mol}\right)} \quad (2)$$

and

$$n_{CO_2} = \frac{V_1(L) \rho \left(\frac{g}{L}\right)}{M_{CO_2} \left(\frac{g}{mol}\right)} \quad (3)$$

where n_{solute} and n_{CO_2} are moles of solute (favipiravir) and CO₂ in the sampling loop, respectively, C_s denotes the solute concentration (g/L) in the collection vial as obtained from the calibration curves. The volumes of the collection vial and sampling loop are $V_s(L) = 5 \times 10^{-3}$ and $V_1(L) = 600 \times 10^{-6}$ respectively. M_s also represents the molecular weight of the solute while M_{CO_2} is the molecular weight of CO₂. The accuracy of the mentioned volumes (500 μ L and 5 mL) was 0.5% and 0.2% respectively.

The equilibrium solubility, S (g/L), of the solute in the SC-CO₂ can be obtained by Eq. (4):

$$S = \rho \frac{M_2}{M_1} \frac{y_2}{(1 - y_2)} \quad (4)$$

3. Modeling studies

In this research, three types of models were considered to correlate the experimental solubility data of Favipiravir in SC-CO₂: (1) EoS-based SRK, (2) empirical density-based models (Chrastil, Garlapati and Madras, Sparks et al., Sodeifian et al., K-J, and Keshmiri et al.), and (3) expanded liquid theory (modified Wilson's model).

3.1. Equation of state-based (EoS) models

For solubility measurements of the solid (component 2) in SC-CO₂ (component 1) under the thermodynamic equilibrium condition, the following equation can be used:

$$y_2 = \frac{P_2^{sub}(T)}{P} \frac{\phi_2^{sat,s}(T)}{\phi_2(T, P, y)} \exp \left[\frac{v_2^s (P - P_2^{sub}(T))}{RT} \right] \quad (5)$$

where P , R , T , $P_2^{sub}(T)$, $\phi_2^{sat,s}(T)$, $\phi_2(T, P, y)$, and v_2^s are pressure, gas constant, temperature, sublimation pressure of the drug, saturation fugacity coefficient of the solute, fugacity coefficient of the solute in supercritical phase, and the solid molar volume, respectively. According to Eq. (5), solubility (y_2) depends on the physicochemical properties of the pure components. Since the physicochemical and critical properties of pharmaceutical compounds are not available in the literature; the group contribution methods were used to determine these properties. Different group contribution methods have been developed to estimate the critical and physicochemical properties of the solid compounds (drug). Table 2 reports the critical and other physicochemical properties of favipiravir. Selection of the proper mixing and combining rules to calculate the thermodynamic characteristics of the mixtures and parameters of the EoS is of crucial importance. In the current work, the quadratic mixing rules was applied for EoS.

3.1.1. Soave–Redlich–Kwong equation

The reduced residual Helmholtz energy of the SRK model can be expressed as follows [21]:

$$P = \frac{RT}{v - b} - \frac{a(T)}{v(v + b)} \quad (6)$$

Where R , T , and v are the universal gas constant, absolute temperature, and molar volume, respectively.

The parameters of a and b depend on the critical and physical properties of pure components and can be determined by the following equation (for a single-component system):

$$a(T) = \frac{0.42747R^2 T_c^2}{P_c} \times \alpha(T_{r,\omega}) \quad (7)$$

$$\alpha(T_{r,\omega}) = [1 + m(1 - T_r^{0.5})]^2 \quad (8)$$

$$m = 0.480 + 1.574\omega - 0.176\omega^2 \quad (9)$$

$$b = \frac{0.08664R T_c}{P_c} \quad (10)$$

The quadratic mixing rules in mole fraction for $a(T)$ and b are used as follows:

$$a(T) = \sum_i \sum_j y_i y_j a_{ij}(T) \quad (11)$$

$$b = \sum_i \sum_j y_i y_j b_{ij} \quad (12)$$

Where $a_{ij}(T)$ and b_{ij} are the cross energetic and the cross-co-volume parameters, respectively. $a_{ij}(T)$ and b_{ij} can be calculated by:

$$a_{ij}(T) = \sqrt{a_{ii}(T)a_{jj}(T)}(1 - k_{ij}) \quad (13)$$

$$b_{ij} = \frac{b_i + b_j}{2} (1 - l_{ij}) \quad (14)$$

3.2. Expanded liquid theory

The density of the supercritical fluid is very close to the typical liquid and its phase can be considered as an expanded liquid [22]. As a result, the thermodynamic phase equilibrium of solid and supercritical fluid can be defined by solid-liquid equilibrium and activity coefficients. The activity coefficients are required to calculate the solid solubility in the supercritical phases. In this regard, the equilibrium between the pure solid and the supercritical phase is expressed as follows [23,24]:

$$f_2^s = f_2^{SCF} = f_2^L \quad (15)$$

Where f_2^s and f_2^{SCF} are the fugacity of the solid solute in the solid phase and the supercritical phase, respectively.

The fugacity of solute in the supercritical phase can be expressed by:

$$f_2^L = \gamma_2 y_2 f_2^{OL} \quad (16)$$

and

$$f_2^{os} = \gamma_2 y_2 f_2^{OL} \quad (17)$$

Where γ_2 is the activity coefficient, y_2 is the mole fraction of solid solubility and f_2^{os} is and the fugacity of the pure solid solute in the expanded liquid phase.

According to Prausnitz et al. [25]:

$$\ln \frac{f_2^{os}}{f_2^{OL}} = \frac{-\Delta H_2^f}{R} \left(\frac{1}{T} - \frac{1}{T_m} \right) - \frac{\Delta Cp}{RT} \left(\frac{T - T_m}{T} \right) + \frac{\Delta Cp}{R} \ln \left(\frac{T}{T_m} \right) \quad (18)$$

The heat capacity terms can be neglected [25], so:

$$y_2 = \frac{1}{\gamma_2} \exp \left(\frac{-\Delta H_2^f}{R} \left(\frac{1}{T} - \frac{1}{T_m} \right) \right) \quad (19)$$

Where ΔH_2^f is the enthalpy of fusion and T_m shows the melting point of the solid (drug). The solid solubility in the supercritical fluid is very low (\sim infinite dilution). Therefore, the activity coefficient of the solid solute is one at infinite dilution. Thus, Eq. (19) becomes:

$$y_2 = \frac{1}{\gamma_2^{os}} \exp \left[\frac{-\Delta H_2^f}{R} \left(\frac{1}{T} - \frac{1}{T_m} \right) \right] \quad (20)$$

3.2.1. Modified Wilson model

Wilson equation can be utilized for determining the activity coefficient of the solid solute at infinite dilution. This equation consists of two parts, a combinatorial contribution based on Flory's theory, and a term based on the Gibbs excess energy, which can be written as follows [23]:

$$\frac{G^E}{RT} = - \sum_i x_i \ln \left(\sum_j x_j \Lambda_{ij} \right) \quad (21)$$

Where G^E is the excess Gibbs energy, and Λ_{12} and Λ_{21} represent adjustable parameters.

$$\ln \gamma_i = - \ln \left(\sum_j x_j \Lambda_{ij} \right) + 1 - \sum_k \frac{x_k \Lambda_{ki}}{\sum_j x_j \Lambda_{kj}} \quad (22)$$

According to the theory proposed by Assael et al., [26], Eq. (22) can be rewritten to the following form:

$$\ln \gamma_2^\infty = 1 - \Lambda_{12} - \ln \Lambda_{21}, \quad (23)$$

where Λ_{12} and Λ_{21} are defined at infinite dilution conditions:

$$\Lambda_{12} = v_2 \rho_c \rho_r \exp \left(- \frac{\lambda'_{12}}{T_r} \right), \quad (24)$$

and

$$\Lambda_{21} = \frac{1}{v_2 \rho_c \rho_r} \exp \left(- \frac{\lambda'_{21}}{T_r} \right) \quad (25)$$

Where ρ_c is the critical density of SCF, ρ_r ($\rho_r = \frac{\rho}{\rho_c}$) represents the reduced density of the SCF, v_2 denotes the molar volume of the solid solute. The dimensionless energies of interaction are as follows:

$$\lambda'_{12} = \frac{\lambda_{12}}{RT_{1c}} \quad (26)$$

and

$$\lambda'_{21} = \frac{\lambda_{21}}{RT_{1c}} \quad (27)$$

To address the effect of high pressures and simplify the prediction process, Wilson model was introduced by an empirical expression that linearly correlates the molar volume and the reduced density [23]:

$$v_2 = \alpha \rho_r + \beta \quad (28)$$

where α , β , λ'_{12} and λ'_{21} are the regressed parameters of the model.

3.3. Semi-empirical density-based models

Density-based correlations are common techniques for modeling solid solubility in SCFs. Empirical models do not require estimation of the physicochemical properties of solid as they only depend on temperature, pressure, and density of SCF (independent variables) as well as several adjustable parameters (constants). In the current work, empirical density-based models (proposed by Chrastil, Garlapati, and Madras, Sparks et al., Sodeifian et al., K-J, and Keshmiri et al.) were applied for correlating the experimental solubility data.

The constants in the empirical models were determined by regression of experimental data. The adjustable parameters were optimized by simulated annealing (MATLAB software). The average absolute relative deviation (AARD%) was used to compare the precision of the model with experimental data which can be defined by:

$$AARD\% = \frac{100}{N_t - Z} \sum_{i=1}^{N_t} \frac{|y_2^{cal} - y_2^{exp}|}{y_2^{exp}} \quad (29)$$

Where Z and N_t are the number of fitted parameters for each model and the number of data points in each set, respectively. As another criterion for comparing different models, R_{adj} has the following expression [27, 28]:

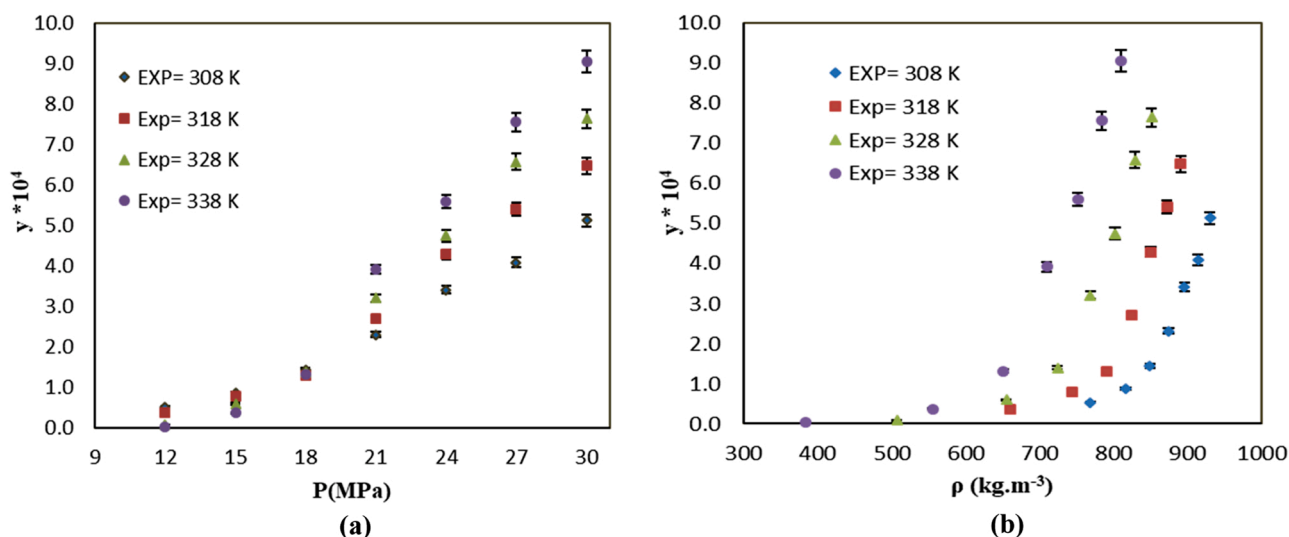
$$R_{adj} = \sqrt{|R^2 - (Q(1 - R^2)/(N - Q - 1))|} \quad (30)$$

Where N shows the number of data points in each set, Q is the number of independent variables in each equation.

Table 3The favipiravir solubility experimental data in SC-CO₂. The y_2 and S are mole fractions and solubility of solute in the SC-CO₂, respectively.^a

Temperature (K)	Pressure (MPa)	Density (kg/m ³)	Binary			
			$y_2 \times 10^4$ (Mole Fraction)	Standard deviation of the mean, SD (\bar{y}) $\times 10^4$	Expanded uncertainty $\times 10^4$	$S \times 10^1$ (Solubility (g/L))
308	12	768.42	0.53	0.014	0.027	1.46
	15	816.06	0.87	0.041	0.047	2.54
	18	848.87	1.44	0.023	0.017	4.37
	21	874.40	2.31	0.023	0.011	7.22
	24	895.54	3.42	0.046	0.014	10.95
	27	913.69	4.09	0.023	0.007	13.35
	30	929.68	5.13	0.069	0.014	17.04
318	12	659.73	0.37	0.041	0.110	0.87
	15	743.17	0.80	0.014	0.018	2.13
	18	790.18	1.30	0.046	0.036	3.67
	21	823.70	2.72	0.047	0.018	8.01
	24	850.10	4.29	0.093	0.022	13.03
	27	872.04	5.41	0.047	0.010	16.86
	30	890.92	6.48	0.116	0.018	20.63
328	12	506.85	0.08	0.001	0.019	0.15
	15	654.94	0.60	0.003	0.008	1.41
	18	724.13	1.39	0.047	0.034	3.60
	21	768.74	3.21	0.070	0.022	8.82
	24	801.92	4.75	0.068	0.015	13.61
	27	828.51	6.58	0.117	0.018	19.48
	30	850.83	7.65	0.092	0.012	23.26
338	12	384.17	0.03	0.008	0.270	0.04
	15	555.23	0.37	0.014	0.037	0.74
	18	651.18	1.32	0.023	0.018	3.07
	21	709.69	3.92	0.070	0.019	9.95
	24	751.17	5.6	0.043	0.009	15.03
	27	783.29	7.57	0.115	0.016	21.19
	30	809.58	9.05	0.163	0.018	26.18

The experimental standard deviation and the experimental standard deviation of the mean (SD) were calculated by $S(y_k) = \sqrt{\frac{\sum_{j=1}^n (y_j - \bar{y})^2}{n-1}}$ and $SD(\bar{y}) = \frac{S(y_k)}{\sqrt{n}}$ respectively. The relative combined standard uncertainty was obtained by $U_{\text{combined}}/y = \sqrt{\sum_{i=1}^N (P_i U(x_i)/x_i)^2}$. The expanded uncertainty U is $k \times U_{\text{combined}}$. ^bStandard uncertainty u are (T) = 0.1 K; u(p) = 0.1 MPa. The relative standard uncertainties are calculated below 0.05 for solubilities and mole fractions. ^c Data from the Span–Wagner equation of state ¹⁸.

**Fig. 2.** The influence of (a) pressure and (b) density of SC-CO₂ on favipiravir solubility at different temperatures.

4. Results and discussion

4.1. Experimental data

Solubility of favipiravir in SC-CO₂ was experimentally measured at the temperature range of 308–338 K and pressure range of 10–30 MPa. Solubility data of favipiravir is collected in Table 3. The SC-CO₂ density

was calculated by Span-Wanger EoS [29]. Furthermore, each data point was repeated three times to increase the reliability of the measurements; relative standard uncertainties were lower than 5%. The expanded uncertainty with the mole fractions is also reported in Table 3.

Fig. 2 shows the mole fraction solubility of favipiravir vs. pressure and density at different temperatures. In general, the density of SC-CO₂ and its solvating power increased with increasing the pressure.

Table 4Review of some articles on the crossover points of various pharmaceutical compound in SC-CO₂.

Compound	Pressure range (MPa)	Temperature range (K)	Crossover (MPa)	Mole fraction (y)	Ref
Clobetasol Propionate (C ₂₅ H ₃₂ ClFO ₅)	15.5–30.5	315–345	24.5	1 × 10 ⁻⁶ to 2.1 × 10 ⁻⁵	[30]
Desoxycorticosterone acetate (C ₂₁ H ₃₀ O ₃)	15.5–30.5	315–345	24.5	5 × 10 ⁻⁶ to 1.03 × 10 ⁻⁴	[30]
Esomeprazole (C ₁₇ H ₁₉ N ₃ O ₃ S)	12–27	308.2–338.2	22	1.11 × 10 ⁻⁵ to 9.10 × 10 ⁻⁴	[31]
Amiodarone hydrochloride (C ₂₅ H ₂₉ I ₂ NO ₃ ·HCl)	12–30	313.2–343.2	19	2.510 × 10 ⁻⁵ to 1.012 × 10 ⁻³	[32]
Ketotifen fumarate (C ₂₃ H ₂₃ NO ₅ S)	12–30	308.2–338.2	20	2.11 × 10 ⁻⁵ to 1.07 × 10 ⁻³	[33]
Aprepitant (C ₂₃ H ₂₁ F ₇ N ₄ O ₃)	12–33	308.15–338.15	15–18	4.50 × 10 ⁻⁶ to 7.67 × 10 ⁻⁵	[34]
Imatinib mesylate (C ₃₀ H ₃₅ N ₇ O ₄ S)	12–27	308.2–338.2	18–21	1.0 × 10 ⁻⁷ to 4.4 × 10 ⁻⁶	[35]
Coumarin-7 (C ₂₀ H ₁₉ N ₃ O ₂)	9–33	308–338	13–16	4.15 × 10 ⁻⁶ to 1.00 × 10 ⁻⁵	[36]
Loratadine (C ₂₂ H ₂₃ N ₂ O ₂ Cl)	12–27	308.15–338.15	18–21	4.50 × 10 ⁻⁶ to 1.30 × 10 ⁻³	[37]
Cefixime trihydrate (C ₁₆ H ₁₅ N ₅ O ₇ S ₂ ·3 H ₂ O)	18.3–33.5	308–328	NO	1.6 × 10 ⁻⁷ to 3.02 × 10 ⁻⁷	[38]
Oxymetholone (C ₂₁ H ₃₂ O ₃)	18.3–33.5	308–328	18	1.6 × 10 ⁻⁵ to 1.49 × 10 ⁻⁴	[38]
Atorvastatin (C ₃₃ H ₃₃ FN ₂ O ₄)	12.16–35.46	308–348	17	1.12 × 10 ⁻⁶ to 1.45 × 10 ⁻³	[39]
Simvastatin (C ₂₅ H ₃₈ O ₅)	12.16–35.46	308–348	17	2 × 10 ⁻⁶ to 5.35 × 10 ⁻⁴	[39]
Lovastatin (C ₂₄ H ₃₆ O ₅)	12.16–35.46	308–348	17	1.10 × 10 ⁻⁵ to 1.14 × 10 ⁻⁴	[39]
Rosuvastatin (C ₂₂ H ₂₈ FN ₂ O ₅)	12.16–35.46	308–348	17	3 × 10 ⁻⁶ to 2.44 × 10 ⁻⁴	[39]
Fluvastatin (C ₂₄ H ₂₆ FNO ₄)	12.16–35.46	308–348	17	5 × 10 ⁻⁶ to 6 × 10 ⁻⁴	[39]
Azithromycin (C ₃₈ H ₇₂ N ₂ O ₁₂)	12.2–35.5	308–348	13.8–14	6.9 × 10 ⁻⁵ to 2.73 × 10 ⁻⁴	[40]
Erythromycin (C ₃₇ H ₆₇ NO ₁₃)	12.2–35.5	308–348	16.8–17	4.3 × 10 ⁻⁵ to 3.12 × 10 ⁻⁴	[40]
Clindamycin (C ₁₈ H ₃₃ ClN ₂ O ₅ S)	12.2–35.5	308–348	14.8–15.2	1.77 × 10 ⁻⁴ to 1.146 × 10 ⁻³	[40]
Clarithromycin (C ₃₈ H ₆₉ NO ₁₃)	12.2–35.5	308–348	15–15.2	1.31 × 10 ⁻⁴ to 3.28 × 10 ⁻⁴	[40]
Loxoprofen (C ₁₅ H ₁₈ O ₃)	12–40	308–338	20	1.04 × 10 ⁻⁵ to 1.28 × 10 ⁻³	[41]
Cyproheptadine (C ₂₁ H ₂₁ N)	16–40	308–338	20	3.35 × 10 ⁻⁵ to 3.09 × 10 ⁻³	[42]
2,4,7-Triamino-6-phenylpteridine (Triamterene) (C ₁₃ H ₁₃ N ₇)	12–27	308–338	19.2–19.5	0.03 × 10 ⁻⁵ to 2.89 × 10 ⁻⁵	[43]
Tolmetin (C ₁₅ H ₁₅ NO ₃)	12–40	308–338	16	5.00 × 10 ⁻⁵ to 2.59 × 10 ⁻³	[44]
Busulfan (C ₆ H ₁₄ O ₆ S ₂)	12–40	308–338	16	3.27 × 10 ⁻⁵ to 8.65 × 10 ⁻⁴	[45]
Sunitinib malate (C ₂₆ H ₃₃ FN ₄ O ₇)	12–27	308–338	NO	0.5 × 10 ⁻⁵ to 8.56 × 10 ⁻⁵	[46]
Fenoprofen (C ₁₅ H ₁₄ O ₃)	12–40	308–338	16	2.01 × 10 ⁻⁵ to 4.20 × 10 ⁻³	[47]
Azathioprine (C ₉ H ₇ N ₇ O ₂ S)	12–27	308–338	12–15	0.27 × 10 ⁻⁵ to 1.83 × 10 ⁻⁵	[48]
Sorafenib tosylate (C ₂₈ H ₂₄ ClF ₃ N ₄ O ₆ S)	12–27	308–338	NO	0.68 × 10 ⁻⁶ to 12.57 × 10 ⁻⁶	[49]
spiroidolinonaphthoxazine photochromic dye (1,3-dihydro-3,3-dimethyl-1-isopropyl-6-(2,3)-(dihydroindole-1-yl)spiro[2 H-indole-2,3 – 3 H-naphtho [2,1-b][1,4]oxazine])	10–26	308–328	17	2.2 × 10 ⁻⁷ to 5.05 × 10 ⁻⁶	[50]
Flurbiprofen (C ₁₅ H ₁₃ FO ₂)	8–25	303–323	12	2.170 × 10 ⁻⁵ to 19.683 × 10 ⁻⁵	[51]
Artemisinin (C ₁₅ H ₂₂ O ₅)	10–25	303–328	13–17	10 ⁻⁴ to 10 ⁻³	[52]
Juglone (5-hydroxy-1,4-naphthoquinone) (C ₁₀ H ₆ O ₃)	9.2–24.4	308.2–328.2	21–22	2.0 × 10 ⁻⁵ to 1.6 × 10 ⁻³	[53]
Diflunisal (5-(2,4-difluorophenyl)-2-hydroxybenzoic acid) (C ₁₃ H ₈ F ₂ O ₃)	9–25	308.2–328.2	15	0.54 × 10 ⁻⁶ to 8.07 × 10 ⁻⁶	[54]
Norfloxacin (C ₁₆ H ₁₈ FN ₃ O ₃)	10–30.3	308.2–328.2	NO	1.4 × 10 ⁻⁶ to 24.4 × 10 ⁻⁶	[55]
Ofloxacin (C ₁₈ H ₂₁ ClFN ₃ O ₄)	10–30.3	308.2–328.2	NO	0.4 × 10 ⁻⁶ to 1.3 × 10 ⁻⁶	[55]
Meloxicam sodium (C ₁₄ H ₁₂ N ₃ NaO ₄ S ₂)	14.9–25.5	303–323	15–17	4.41 × 10 ⁻⁶ to 12.76 × 10 ⁻⁶	[56]
CIBA photoinitiator Irgacure® 2959 2-Hydroxy-4'-(2-hydroxyethoxy)-2-methylpropiophenone (C ₁₂ H ₁₆ O ₄)	10–26	308.2–328.2	14	5.17 × 10 ⁻⁶ to 2.83 × 10 ⁻⁴	[57]

Therefore, favipiravir solubility in SC-CO₂ rose with increasing pressure (Table 3 and Fig. 2). As indicated in Fig. 2, at the pressure range of 12–18 MPa, the solubility of favipiravir in SC-CO₂ decreased with increasing the temperature. At pressures below 18 MPa, favipiravir solubility showed a decremental trend with increasing temperature. Above this pressure (18 MPa), the solubility increased with elevating the temperature. The mentioned trend can be also observed in Fig. 2, where the solubility curve showed the crossover region between 15 and 18 MPa. At pressures lower than the crossover region, the density effect is predominant and as a result, the solubility increases with decreasing temperature. However, at pressures above the crossover point, the vapor pressure of the solution was the main factor and the solubility increased at higher temperatures. The crossover point of various pharmaceutical compounds in SC-CO₂ have been investigated by some other researchers, that crossover point of some of these compounds was reported in Table 4.

The crossover pressure was investigated by several articles which proposed some methods to predict the crossover pressure region [58–61]. Investigation of these methods showed the crossover region depends on the critical properties of solutes, sublimation pressure, enthalpy of sublimation, partial molar enthalpy, and molar volume of the solute. Minimum and maximum favipiravir solubility were seen at the temperature of 338 K and pressures of 12 and 30, respectively. As indicated in Table 3, the mole fraction of favipiravir in the binary system (favipiravir-SC-CO₂) ranged in 3.0 × 10⁻⁶–9.05 × 10⁻⁴. The mole

Table 5Modified Wilson model parameters for solubility of favipiravir in SC-CO₂.

α	β	λ'_{12}	λ'_{21}	AARD%	R _{adj}
-0.000027	0.000929	0.2525	15.021	10.09	0.9658

fraction of drugs in Table 4 shows a wide range of values. These values were reported between 10⁻³ and 10⁻⁷ according to the experimental conditions. The mole fraction of favipiravir also was in this range. The results present that high mole fraction values were obtained in the order of 10⁻⁴. As above mentioned some researchers reported that the solubility of solutes in SC-CO₂ can be dependent on the critical properties of solutes, sublimation pressure values, enthalpy of sublimation, partial molar enthalpy, and molar volume of solute. This experimental data can be used to develop the method for the production of favipiravir nanoparticles using SCF. This information can be also employed for the incorporation of polar co-solvent to increase the solubility.

4.2. Expanded liquid theory - Modified Wilson model

The modified Wilson model was studied to model the favipiravir solubility in SC-CO₂. The modified Wilson model parameters (α , β , λ'_{12} and λ'_{21}) were optimized for binary system favipiravir-SC-CO₂. The results on the solubility of favipiravir in SC-CO₂ are listed in Table 5.

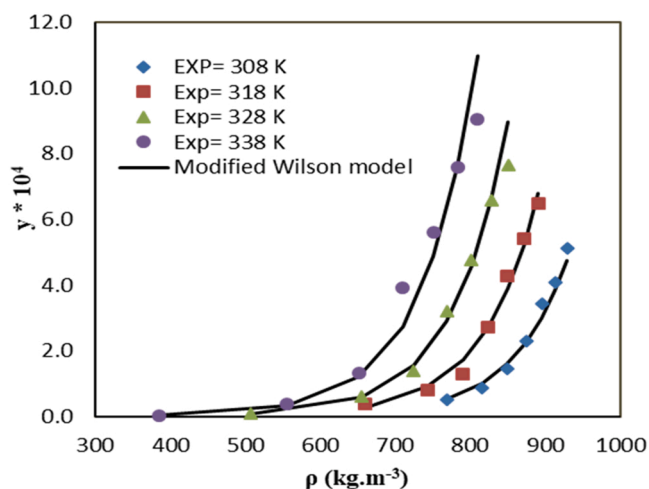


Fig. 3. Comparison of experimental data (point) and calculated (line) solubility of favipiravir in SC-CO₂ based on modified Wilson model.

Table 6
Semi-empirical models.

Name	Formula
Chrastil	$\ln S = a_0 \ln p + a_1 + \frac{a_2}{T}$
K-J	$\ln y_2 = a_0 + a_1 p + \frac{a_2}{T}$
Keshmiri et al.	$\ln y_2 = a_0 + \frac{a_1}{T} + a_2 p^2 + \left(a_3 + \frac{a_4}{T}\right) \ln p$
Sparks et al.	$S_2^* = \frac{\rho M_w \text{ solute } y_2}{p_{r,1}^{a_0 + a_1 p_{r,1} + a_2 p_{r,1}^2}} \exp\left(a_3 + \frac{a_4}{T_r} + \frac{a_5}{T_r^2}\right) S_2^* = \frac{S}{p_{c,1}} S =$
Sodeifian et al.	$\ln y_2 = a_0 + a_1 \frac{p}{T} + a_2 \ln(\rho T) + a_3 (p \ln p) + a_4 p \ln T + a_5 \frac{\ln p}{T}$
Garlapati and Madras	$\ln y_2 = a_0 + (a_1 + a_2 p) \ln p + \frac{a_3}{T} + a_4 \ln(\rho T)$

a $a_0 - a_5$, adjustable parameters of models.

Fig. 3 shows the experimental data and model of solubility of favipiravir in SC-CO₂. As indicated in Fig. 3, the model exhibited a proper agreement with experimental solubility data of favipiravir in SC-CO₂. According to Table 5, the values of AARD% and R_{adj} were 10.09% and 0.9658. Therefore, the modified Wilson model can correlate the solubility of favipiravir at proper accuracy.

4.3. Correlation of the solubility data with semi-empirical models

As presented in Table 6, six empirical density-based models (Chrastil, K-J, Keshmiri et al., Sparks et al., Sodeifian et al., and Garlapati-Madras) were used to correlate favipiravir solubility experimental data in a binary system (favipiravir-SC-CO₂). The results and adjustable parameters of each empirical model are listed in Table 7.

The equation developed by K-J (AARD = 10.55%) presented the best fit compared to the other equation with three parameters namely

Table 7
The correlation results of the favipiravir – CO₂ system provided by semi-empirical models.^a

Model	a_0	a_1	a_2	a_3	a_4	a_5	a_6	AARD%	R_{adj}
Chrastil	10.01	-8267.85	-40.35	–	–	–	–	18.61	0.966
K-J	7.35	-8593.17	0.014	–	–	–	–	10.55	0.957
Keshmiri et al.	-43.11	-4486.03	0.0000129	7.99	-253.79	–	–	15.55	0.954
Sparks et al.,	4.98	2.74	16.41	-29.65	4358.15	11.14	–	11.10	0.976
Sodeifian et al.,	-16.03	-0.00506	1.58	0.0021	0.012	-1177.91	–	13.45	0.966
Garlapati and Madras	-61.13	-8.1	0.0016	-5595.52	9.29	–	–	11.31	0.956

^a $a_0 - a_6$, adjustable parameters of models.

Chrastil (AARD = 18.61%). K-J provided a relationship between the logarithm of the mole fraction of a solute has a linear dependence on the density of the SCF phase. On the other hand, Chrastil described one of the first density-based models, based on the solvato complex formed between the solute and solvent molecules at equilibrium. However, it has some limitations in high solubility [62]. Therefore, the model described by Chrastil underwent several modifications, deriving in different equations like Adachi-Lu [63] and del Valle and Aguilera [64]. Moreover, Sparks et al. combined Adachi-Lu and del Valle- Aguilera models considering the effect of the density in the association number k and the change of the enthalpy of vaporization with the temperature. The results in Table 7 showed that Sparks et al. (AARD = 11.10%) was more adequate than Chrastil model.

Keshmiri et al. introduced a semi-empirical model based on the effect of pressure, density, and temperature. This model is expressed by a linear relationship between the logarithm of the solid solubility and the density of the CO₂ and it has a strong relationship with pressure. Keshmiri's model (AARD= 15.55%) with more parameters, but the fit was worse compared to K-J and better than Chrastil. In this model, the relationship of solubility to pressure, density, and temperature are complicated.

Sodeifian et al. and Garlapati-Madras models were developed by reviewing the laboratory data and models presented. Both of them included more combined terms than K-J, but the AARDs obtained with these models were 13.45% and 11.31% respectively. The main conclusion obtained from Table 7 is that the best models for correlating favipiravir solubility were the equation developed by K-J and Sparks et al."

Furthermore, experimental data and favipiravir solubility calculated by empirical models are compared in Fig. 4. As seen, the models showed satisfactory agreement with experimental data. Using the model, total heat ($\Delta H_{total} = 70.09$ KJ mol⁻¹), vaporization heat ($\Delta H_{vap} = 90.12$ KJ mol⁻¹), and solvation heat ($\Delta H_{sol} = 20.04$ KJ mol⁻¹) can be calculated for binary system.

4.4. Solubility correlation with EoS model

In this study, the SRK EoS with quadratic mixing rules was employed. Interaction parameters (k_{ij} , l_{ij}) are used to calculate the parameters of the SRK equation for the binary system. As previously mentioned, different group contribution (GC) methods are used to calculate the physico-chemical and critical properties of solids (drug), which can affect the correlation results (AARD) for solubility data in SC-CO₂ by EoS, but in many cases the results were not significantly different [65]. In the current research, the Ambrose-Walton equation [66], Immirzi and Perini [67], Edmister [66] and Marrero and Gani [68], methods were applied to determine the sublimation pressure, solid molar volume, acentric factor, critical temperature and pressure, respectively. The results of estimating of drug properties are presented in Table 2.

Moreover, interaction parameters can be written as a function of temperature:

$$l_{ij} = AT + B \quad (32)$$

$$k_{ij} = CT + D \quad (33)$$

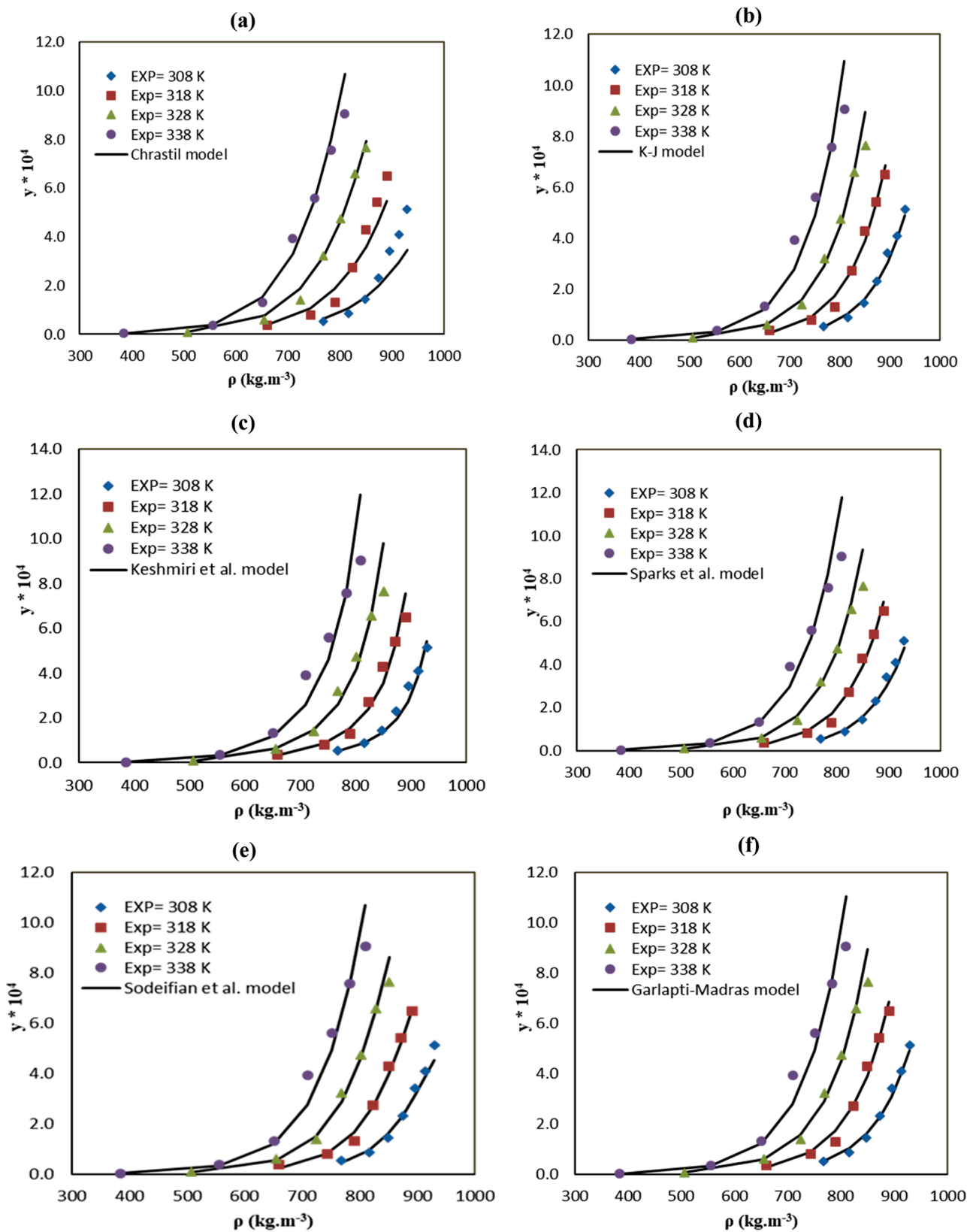
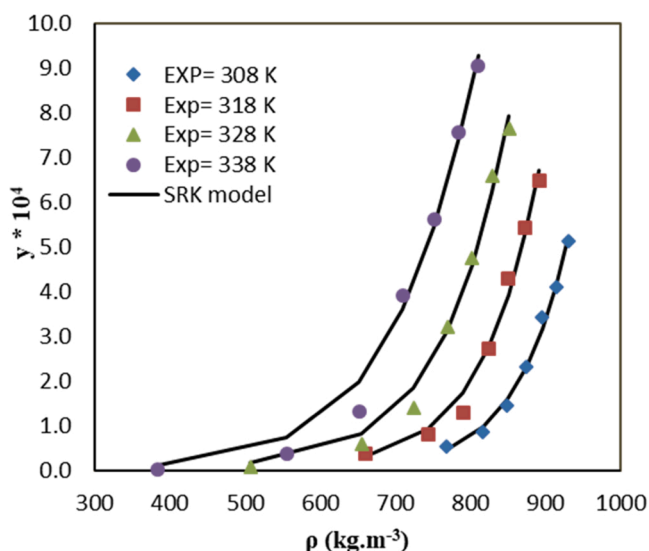
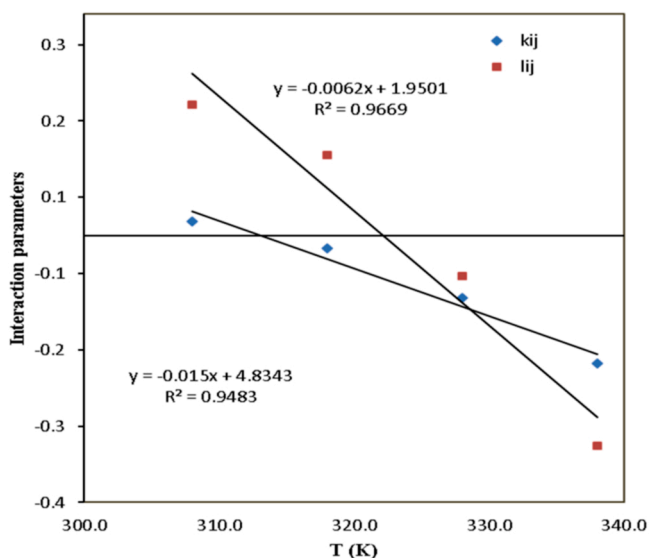


Fig. 4. Comparison of experimental (points) and calculated (line) values of favipiravir solubility based on the (a) Chrastil, (b) K-J, (c) Keshmiri (d) Sparks et al., (e) Sodeifian et al., and (f) Garlapati and Madras models at different temperatures.

Table 8Correlation results of the SRK for solubility of favipiravir in SC-CO₂, interaction parameters.

Model	Parameter	T = 308 K	T = 318 K	T = 328 K	T = 338 K
SRK	k_{12}	0.018	-0.0168	-0.0818	-0.168
	l_{12}	0.1717	0.1052	-0.053	-0.2758
	AARD	6.08	11.59	15.04	17.65
	R_{adj}	0.996	0.986	0.975	0.965

**Fig. 5.** Comparison of experimental and calculated solubilities of favipiravir base on SRK- with quadratic mixing rules EoS.**Fig. 6.** The influence of temperature on the binary interaction parameters for the favipiravir SC-CO₂ system, SRK model.

The corresponding values of interaction parameters were optimized by the simulated annealing (SA) method. The correlation results obtained with the SRK-EoS and quadratic mixing rules at four temperatures are reported in Table 8. According to AARD% values in Table 8, the interaction parameters were calculated with acceptable accuracy. However, it can be said that the accuracy of the data obtained at low temperatures (308 K) is higher than those determined at high

temperatures (338 K). Fig. 5 shows the experimental solubility of favipiravir in SC-CO₂ at four temperatures (308, 318, 328, and 338 K) and those predicted by SRK-EoS. As indicated in Fig. 5, the SRK EoS with quadratic mixing rules was capable of correlating solubility data. The coefficients of A, B, C, and D (Eq. (33), (34)) were calculated via linear regression analysis (Fig. 6).

5. Conclusion

Proper knowledge of drug's solubility in a supercritical fluid is essential in the production of pharmaceutical micro and nanoparticles using supercritical fluids. In this study, the solubility of favipiravir in SC-CO₂ was explored at the temperature range 308 – 338 K and pressure range 12–30 MPa. The solubility of favipiravir in SC-CO₂ varying from 0.004 to 2.618 g/L was obtained. The minimum and maximum values for favipiravir solubility were observed in the temperature of 338 K and pressures of 12 and 30 MPa. After experimental measurement of the solubility, three models including expanded liquid theory (modified Wilson model), semi-empirical density-based models (Chrastil, K-J, Keshmiri et al., Sparks et al., Sodeifian et al., and Garlapati- Madras), and equation of state (SRK with quadratic mixing rules) were used to correlate the generated solubility data. According to the results, K-J (AARD% = 10.55), Sparks et al. (AARD% = 11.1), and Garlapati and Madras (AARD% = 11.31) showed a better agreement with solubility data of favipiravir compared to SRK model (12.59%). Comparison of the models showed that the best model for correlating favipiravir solubility is the modified Wilson (AARD% = 10.09) and K-J (AARD% = 10.55).

Declaration of Competing Interest

The authors declare that they have no known competing financial interests or personal relationships that could have appeared to influence the work reported in this paper.

Acknowledgements

The authors herein express their thanks to the Laboratory of Supercritical Fluids of Dr Sajadian for providing experimental facilities.

References

- [1] T. Manabe, D. Kambayashi, H. Akatsu, K. Kudo, Favipiravir for the treatment of patients with COVID-19: a systematic review and meta-analysis, *BMC Infect. Dis.* 21 (2021) 1–13, <https://doi.org/10.1186/s12879-021-06164-x>.
- [2] C. Chen, J. Huang, Z. Cheng, J. Wu, S. Chen, Y. Zhang, B. Chen, M. Lu, Y. Luo, J. Zhang, Favipiravir versus arbidol for COVID-19: a randomized clinical trial, *MedRxiv* (2020), <https://doi.org/10.1101/2020.03.17.20037432>.
- [3] S. Joshi, J. Parkar, A. Ansari, A. Vora, D. Talwar, M. Tiwaskar, S. Patil, H. Barkate, Role of favipiravir in the treatment of COVID-19, *J. Glob. Infect. Dis.* (2020), <https://doi.org/10.1016/j.jgid.2020.10.069>.
- [4] M. Abd Elkodous, S. Olojede, M. Morsi, G.S. El-Sayyad, Nanomaterial-based drug delivery systems as promising carriers for patients with COVID-19, *RSC Adv.* 11 (2021) 26463–26480, <https://doi.org/10.1039/d1ra04835j>.
- [5] U. Agrawal, R. Raju, Z.F. Udawadia, Favipiravir: a new and emerging antiviral option in COVID-19, *Med J. Armed Forces India* 76 (2020) 370–376, <https://doi.org/10.1016/j.mjafi.2020.08.004>.
- [6] R.M. Moshikur, M.K. Ali, R. Wakabayashi, M. Moniruzzaman, M. Goto, Favipiravir-based ionic liquids as potent antiviral drugs for oral delivery: synthesis, solubility, and pharmacokinetic evaluation, *Mol. Pharm.* 18 (2021) 3108–3115, <https://doi.org/10.1021/acs.molpharmaceut.1c00324>.
- [7] N.S. Ardestani, M. Amani, Production of anthraquinone violet 3RN nanoparticles via the GAS process: optimization of the process parameters using Box-Behnken Design, *Dyes Pigm* 193 (2021), 109471, <https://doi.org/10.1016/j.dyepig.2021.109471>.
- [8] N.S. Ardestani, M. Amani, L. Moharrery, Determination of anthraquinone violet 3RN solubility in supercritical carbon dioxide with/without co-solvent: experimental data and modeling (empirical and thermodynamic models), *Chem. Eng. Res. Des.* 159 (2020) 529–542, <https://doi.org/10.1016/j.cherd.2020.04.026>.
- [9] N.S. Ardestani, N.Y. Majid, M. Amani, Experimental measurement and thermodynamic modeling of capecitabine (an anticancer drug) solubility in supercritical carbon dioxide in a ternary system: effect of different cosolvents, *J. Chem. Eng. Data* 65 (2020) 4762–4779, <https://doi.org/10.1021/acs.jced.0c00183>.

- [10] M. Amani, N.S. Ardestani, N.Y. Majd, Utilization of supercritical CO₂ gas antisolvent (GAS) for production of Capecitabine nanoparticles as anti-cancer drug: analysis and optimization of the process conditions, *J. CO₂ Util.* 46 (2021), 101465, <https://doi.org/10.1016/j.jcou.2021.101465>.
- [11] A. Martín, M.J. Cocero, Micronization processes with supercritical fluids: fundamentals and mechanisms, *Adv. Drug Deliv. Rev.* 60 (2008) 339–350, <https://doi.org/10.1016/j.addr.2007.06.019>.
- [12] Z.E. Knez, D. Čor, M.A. Knez Hrncič, Solubility of solids in sub-and supercritical fluids: a review 2010–2017, *J. Chem. Eng. Data.* 63 (2017) 860–884, <https://doi.org/10.1021/acs.jced.7b00778>.
- [13] S. Zabihi, A. Khoshmaram, M. Pishnamazi, F. Borousan, A.Z. Hezave, A. Marjani, R. Pelalak, T.A. Kurniawan, S. Shirazian, Thermodynamic study on solubility of brain tumor drug in supercritical solvent: temozolomide case study, *J. Mol. Liq.* 321 (2021), 114926, <https://doi.org/10.1016/j.molliq.2020.114926>.
- [14] S.K. Misra, K. Pathak, Supercritical fluid technology for solubilization of poorly water soluble drugs via micro-and nano-sized particle generation, *ADMET DMPK* 8 (2020) 355–374, <https://doi.org/10.5599/admet.811>.
- [15] H. Liu, B.-Q. Chen, Y.-J. Pan, C.-P. Fu, R.K. Kankala, S.-B. Wang, A.-Z. Chen, Role of supercritical carbon dioxide (scCO₂) in fabrication of inorganic-based materials: a green and unique route, *Sci. Technol. Adv. Mater.* 22 (2021) 695–717, <https://doi.org/10.1080/14686996.2021.1955603>.
- [16] R.K. Kankala, P.-Y. Xu, B.-Q. Chen, S.-B. Wang, A.-Z. Chen, Supercritical fluid (SCF)-assisted fabrication of carrier-free drugs: an eco-friendly welcome to active pharmaceutical ingredients (APIs), *Adv. Drug Deliv. Rev.* 176 (2021), 113846, <https://doi.org/10.1016/j.addr.2021.113846>.
- [17] Z. Akbari, M. Amanlou, J. Karimi-Sabet, A. Golestani, M. Shariaty Niassar, Application of supercritical fluid[†] technology for preparation of drug loaded[†] solid lipid nanoparticles, *Int. J. Nanosci. Nanotechnol.* 16 (2020) 13–33.
- [18] L.K. Bin, A.K. Janakiraman, F.S. Abd Razak, A.H. Uddin, M.Z.I. Sarker, L.C. Ming, B.H. Goh, Supercritical fluid technology and its pharmaceutical applications: a revisit with two decades of progress, *Indian J. Pharm. Educ. Res.* 54 (2020) s1–s3, <https://doi.org/10.5530/ijper.54.2s.56>.
- [19] D.L. Sparks, R. Hernandez, L. Estévez, Evaluation of density-based models for the solubility of solids in supercritical carbon dioxide and formulation of a new model, *Chem. Eng. Sci.* 63 (2008) 4292–4301, <https://doi.org/10.1016/j.ces.2008.05.031>.
- [20] G. Sodeifian, S.A. Sajadian, N.S. Ardestani, Determination of solubility of Aprepitant (an antiemetic drug for chemotherapy) in supercritical carbon dioxide: empirical and thermodynamic models, *J. Supercrit. Fluids* 128 (2017) 102–111, <https://doi.org/10.1016/j.supflu.2017.05.019>.
- [21] G. Soave, Equilibrium constants from a modified Redlich-Kwong equation of state, *Chem. Eng. Sci.* 27 (1972) 1197–1203, [https://doi.org/10.1016/0009-2509\(72\)80096-4](https://doi.org/10.1016/0009-2509(72)80096-4).
- [22] H. Higashi, Y. Iwai, Y. Arai, Solubilities and diffusion coefficients of high boiling compounds in supercritical carbon dioxide, *Chem. Eng. Sci.* 56 (2001) 3027–3044, [https://doi.org/10.1016/s0009-2509\(01\)00003-3](https://doi.org/10.1016/s0009-2509(01)00003-3).
- [23] L. Nasri, Modified Wilson's model for correlating solubilities in supercritical fluids of some polycyclic aromatic solutes, *Polycycl. Aroma Compd.* 38 (2018) 244–256, <https://doi.org/10.1080/10406638.2016.1200636>.
- [24] L. Nasri, S. Bensaad, Z. Bensetiti, Correlation and prediction of the solubility of solid solutes in chemically diverse supercritical fluids based on the expanded liquid theory, *Adv. Chem. Eng.* 3 (2013) 255–273, <https://doi.org/10.4236/aces.2013.34033>.
- [25] J.M. Prausnitz, R.N. Lichtenthaler, E.G. de Azevedo, *Molecular thermodynamics of fluid-phase equilibria*, Pearson Education, 1998.
- [26] M.J. Assael, J.M. Trusler, T.F. Tsolakis, *Thermophysical properties of fluids: an introduction to their prediction*, World Scientific, 1996.
- [27] A. Jouyban, M. Rehman, B.Y. Shekunov, H.K. Chan, B.J. Clark, P. York, Solubility prediction in supercritical CO₂ using minimum number of experiments, *J. Pharm. Sci.* 91 (2002) 1287–1295, <https://doi.org/10.1002/jps.10127>.
- [28] C. Garlapati, G. Madras, New empirical expressions to correlate solubilities of solids in supercritical carbon dioxide, *Thermochim. Acta* 500 (2010) 123–127, <https://doi.org/10.1016/j.tca.2009.12.004>.
- [29] R. Span, W. Wagner, A new equation of state for carbon dioxide covering the fluid region from the triple-point temperature to 1100 K at pressures up to 800 MPa, *J. Phys. Chem. Ref. Data* 25 (1996) 1509–1596, <https://doi.org/10.1063/1.555991>.
- [30] K. Keshmiri, A. Vatanara, Y. Yamini, Development and evaluation of a new semi-empirical model for correlation of drug solubility in supercritical CO₂, *Fluid Ph. Equilibria.* 363 (2014) 18–26, <https://doi.org/10.1016/j.fluid.2013.11.013>.
- [31] G. Sodeifian, R. Detakhsheshpour, S.A. Sajadian, Experimental study and thermodynamic modeling of Esomeprazole (proton-pump inhibitor drug for stomach acid reduction) solubility in supercritical carbon dioxide, *J. Supercrit. Fluids* 154 (2019), 104606, <https://doi.org/10.1016/j.supflu.2019.104606>.
- [32] G. Sodeifian, S.A. Sajadian, F. Razmimanesh, Solubility of an antiarrhythmic drug (amiodarone hydrochloride) in supercritical carbon dioxide: experimental and modeling, *Fluid Ph. Equilibria.* 450 (2017) 149–159, <https://doi.org/10.1016/j.fluid.2017.07.015>.
- [33] G. Sodeifian, N.S. Ardestani, S.A. Sajadian, H.S. Panah, Measurement, correlation and thermodynamic modeling of the solubility of Ketotifen fumarate (KTF) in supercritical carbon dioxide: evaluation of PCP-SAFT equation of state, *Fluid Ph. Equilibria* 458 (2018) 102–114, <https://doi.org/10.1016/j.fluid.2017.11.016>.
- [34] G. Sodeifian, S.A. Sajadian, N.S. Ardestani, Determination of solubility of Aprepitant (an antiemetic drug for chemotherapy) in supercritical carbon dioxide: empirical and thermodynamic models, *J. Supercrit. Fluids* 128 (2017) 102–111, <https://doi.org/10.1016/j.supflu.2017.05.019>.
- [35] G. Sodeifian, F. Razmimanesh, S.A. Sajadian, Solubility measurement of a chemotherapeutic agent (Imatinib mesylate) in supercritical carbon dioxide: assessment of new empirical model, *J. Supercrit. Fluids* 146 (2019) 89–99, <https://doi.org/10.1016/j.supflu.2019.01.006>.
- [36] G. Sodeifian, N.S. Ardestani, S.A. Sajadian, H.S. Panah, Experimental measurements and thermodynamic modeling of Coumarin-7 solid solubility in supercritical carbon dioxide: production of nanoparticles via RESS method, *Fluid Ph. Equilibria.* 483 (2019) 122–143, <https://doi.org/10.1016/j.fluid.2018.11.006>.
- [37] G. Sodeifian, F. Razmimanesh, S.A. Sajadian, H.S. Panah, Solubility measurement of an antihistamine drug (Loratadine) in supercritical carbon dioxide: assessment of qCPA and PCP-SAFT equations of state, *Fluid Ph. Equilibria.* 472 (2018) 147–159, <https://doi.org/10.1016/j.fluid.2018.05.018>.
- [38] M. Khamda, M.H. Hosseini, M. Rezaee, Measurement and correlation solubility of cefixime trihydrate and oxymetholone in supercritical carbon dioxide (CO₂), *J. Supercrit. Fluids* 73 (2013) 130–137, <https://doi.org/10.1016/j.supflu.2012.09.006>.
- [39] M. Hojjati, Y. Yamini, M. Khajeh, A. Vatanara, Solubility of some statin drugs in supercritical carbon dioxide and representing the solute solubility data with several density-based correlations, *J. Supercrit. Fluids* 41 (2007) 187–194, <https://doi.org/10.1016/j.supflu.2006.10.006>.
- [40] H. Astiabi, Y. Yamini, F. Latifeh, A. Vatanara, Solubilities of four macrolide antibiotics in supercritical carbon dioxide and their correlations using semi-empirical models, *J. Supercrit. Fluids* 104 (2015) 62–69, <https://doi.org/10.1016/j.supflu.2015.05.018>.
- [41] S. Zabihi, S.H. Esmaeili-Faraj, F. Borousan, A.Z. Hezave, S. Shirazian, Loxoprofen solubility in supercritical carbon dioxide: experimental and modeling approaches, *J. Chem. Eng. Data.* 65 (2020) 4613–4620, <https://doi.org/10.1021/acs.jced.0c00470>.
- [42] M. Lashkarbolooki, A.Z. Hezave, Y. Rahnama, R. Ozlati, H. Rajaei, F. Esmailzadeh, Solubility of cyproheptadine in supercritical carbon dioxide; experimental and modeling approaches, *J. Supercrit. Fluids* 84 (2013) 13–19, <https://doi.org/10.1016/j.supflu.2013.09.004>.
- [43] G. Sodeifian, C. Garlapati, S.M. Hazaveie, F. Sodeifian, Solubility of 2, 4, 7-Triamino-6-phenylpteridine (Triamterene, Diuretic Drug) in supercritical carbon dioxide: experimental data and modeling, *J. Chem. Eng. Data* 65 (2020) 4406–4416, <https://doi.org/10.1021/acs.jced.0c00268>.
- [44] M. Pishnamazi, S. Zabihi, P. Sarafzadeh, F. Borousan, A. Marjani, R. Pelalak, S. Shirazian, Using static method to measure tolmetin solubility at different pressures and temperatures in supercritical carbon dioxide, *Sci. Rep.* 10 (2020) 1–7, <https://doi.org/10.1038/s41598-020-76330-9>.
- [45] M. Pishnamazi, S. Zabihi, S. Jamsheidian, H.Z. Hezaveh, A.Z. Hezave, S. Shirazian, Measuring solubility of a chemotherapeutic-anti cancer drug (busulfan) in supercritical carbon dioxide, *J. Mol. Liq.* 317 (2020), 113954, <https://doi.org/10.1016/j.molliq.2020.113954>.
- [46] G. Sodeifian, F. Razmimanesh, S.A. Sajadian, Prediction of solubility of sunitinib malate (an anti-cancer drug) in supercritical carbon dioxide (SC-CO₂): experimental correlations and thermodynamic modeling, *J. Mol. Liq.* 297 (2020), 111740, <https://doi.org/10.1016/j.molliq.2019.111740>.
- [47] S. Zabihi, Y. Rahnama, A. Sharafi, F. Borousan, A. Zeinolabedini Hezave, S. Shirazian, Experimental solubility measurements of fenoprofen in supercritical carbon dioxide, *J. Chem. Eng. Data.* 65 (2020) 1425–1434, <https://doi.org/10.1021/acs.jced.9b00861>.
- [48] G. Sodeifian, F. Razmimanesh, N.S. Ardestani, S.A. Sajadian, Experimental data and thermodynamic modeling of solubility of Azathioprine, as an immunosuppressive and anti-cancer drug, in supercritical carbon dioxide, *J. Mol. Liq.* 299 (2020), 112179, <https://doi.org/10.1016/j.molliq.2019.112179>.
- [49] G. Sodeifian, F. Razmimanesh, S.A. Sajadian, S.M. Hazaveie, Experimental data and thermodynamic modeling of solubility of Sorafenib tosylate, as an anti-cancer drug, in supercritical carbon dioxide: Evaluation of Wong-Sandler mixing rule, *J. Chem. Thermodyn.* 142 (2020), 105998, <https://doi.org/10.1016/j.jct.2019.105998>.
- [50] P. Coimbra, M. Gil, C. Duarte, B.M. Heron, H. De Sousa, Solubility of a spiroindolinonaphthoxazine photochromic dye in supercritical carbon dioxide: experimental determination and correlation, *Fluid Ph. Equilibria* 238 (2005) 120–128, <https://doi.org/10.1016/j.fluid.2005.09.024>.
- [51] A.R.C. Duarte, P. Coimbra, H.C. de Sousa, C.M. Duarte, Solubility of flurbiprofen in supercritical carbon dioxide, *J. Chem. Eng. Data.* 49 (2004) 449–452, <https://doi.org/10.1021/je034099b>.
- [52] P. Coimbra, M.R. Blanco, H.S. Costa Silva, M.H. Gil, H.C. de Sousa, Experimental determination and correlation of artemisinin's solubility in supercritical carbon dioxide, *J. Chem. Eng. Data* 51 (2006) 1097–1104, <https://doi.org/10.1021/je060015y>.
- [53] S. Marceneiro, P. Coimbra, M.E. Braga, A.M. Dias, H.C. de Sousa, Measurement and correlation of the solubility of juglone in supercritical carbon dioxide, *Fluid Ph. Equilibria.* 311 (2011) 1–8, <https://doi.org/10.1016/j.fluid.2011.08.024>.
- [54] P. Coimbra, D. Fernandes, M.H. Gil, H.C. de Sousa, Solubility of diflunisal in supercritical carbon dioxide, *J. Chem. Eng. Data* 53 (2008) 1990–1995, <https://doi.org/10.1021/je800384h>.
- [55] R. Chim, S. Marceneiro, M.E. Braga, A.M. Dias, H.C. de Sousa, Solubility of norfloxacin and ofloxacin in supercritical carbon dioxide, *Fluid Ph. Equilibria.* 331 (2012) 6–11, <https://doi.org/10.1016/j.fluid.2012.06.023>.
- [56] H.C. de Sousa, M.S. Costa, P. Coimbra, A.A. Matias, C.M. Duarte, Experimental determination and correlation of meloxicam sodium salt solubility in supercritical carbon dioxide, *J. Supercrit. Fluids* 63 (2012) 40–45, <https://doi.org/10.1016/j.supflu.2011.12.004>.

- [57] P. Coimbra, D. Fernandes, P. Ferreira, M.H. Gil, H.C. de Sousa, Solubility of Irgacure® 2959 photoinitiator in supercritical carbon dioxide: experimental determination and correlation, *J. Supercrit. Fluids* 45 (2008) 272–281, <https://doi.org/10.1016/j.supflu.2008.01.014>.
- [58] S.S.V. de Melo, G.M.N. Costa, A. Viana, F. Pessoa, Solid pure component property effects on modeling upper crossover pressure for supercritical fluid process synthesis: a case study for the separation of Annatto pigments using SC-CO₂, *J. Supercrit. Fluids* 49 (2009) 1–8, <https://doi.org/10.1016/j.supflu.2008.12.006>.
- [59] Y. Budkov, A. Kolesnikov, D. Ivlev, N. Kalikin, M. Kiselev, Possibility of pressure crossover prediction by classical dft for sparingly dissolved compounds in SC-CO₂, *J. Mol. Liq.* 276 (2019) 801–805, <https://doi.org/10.1016/j.molliq.2018.12.021>.
- [60] N.N. Kalikin, M.V. Kurskaya, D.V. Ivlev, M.A. Krestyaninov, R.D. Oparin, A. L. Kolesnikov, Y.A. Budkov, A. Idrissi, M.G. Kiselev, Carbamazepine solubility in supercritical CO₂: a comprehensive study, *J. Mol. Liq.* 311 (2020), 113104, <https://doi.org/10.1016/j.molliq.2020.113104>.
- [61] N. Kalikin, R. Oparin, A. Kolesnikov, Y. Budkov, M. Kiselev, A crossover of the solid substances solubility in supercritical fluids: what is it in fact? *J. Mol. Liq.* 334 (2021), 115997 <https://doi.org/10.1016/j.molliq.2021.115997>.
- [62] A. Taberero, E.M.M. del Valle, M.Á. Galán, A comparison between semiempirical equations to predict the solubility of pharmaceutical compounds in supercritical carbon dioxide, *J. Supercrit. Fluids* 52 (2010) 161–174, <https://doi.org/10.1016/j.supflu.2010.01.009>.
- [63] Y. Adachi, B.C.Y. Lu, Supercritical fluid extraction with carbon dioxide and ethylene, *Fluid Ph Equilibria*. 14 (1983) 147–156, [https://doi.org/10.1016/0378-3812\(83\)80120-4](https://doi.org/10.1016/0378-3812(83)80120-4).
- [64] J.M. Del Valle, J.M. Aguilera, An improved equation for predicting the solubility of vegetable oils in supercritical carbon dioxide, *Ind. Eng. Chem. Res.* 27 (1988) 1551–1553, <https://doi.org/10.1021/ie00080a036>.
- [65] G. Sodeifian, R. Drakhsheshpoor, S.A. Sajadian, Experimental study and thermodynamic modeling of Esomeprazole (proton-pump inhibitor drug for stomach acid reduction) solubility in supercritical carbon dioxide, *J. Supercrit. Fluids* 154 (2019), 104606, <https://doi.org/10.1016/j.supflu.2019.104606>.
- [66] B.E. Poling, J.M. Prausnitz, J.P. O'Connell, *The properties of gases and liquids*, McGraw-hill, New York, 2001.
- [67] A. Immirzi, B. Perini, Prediction of density in organic crystals, *Acta Crystallogr A*. 33 (1977) 216–218, <https://doi.org/10.1107/s0567739477000448>.
- [68] J. Marrero, R. Gani, Group-contribution based estimation of pure component properties, *Fluid Ph. Equilibria*. 183 (2001) 183–208, [https://doi.org/10.1016/s0378-3812\(01\)00431-9](https://doi.org/10.1016/s0378-3812(01)00431-9).